

Dynamic Control and Optimization of Distributed Energy Resources in a Microgrid

Trudie Wang, Daniel O'Neill, and Haresh Kamath

Abstract—As we transition toward a power grid that is increasingly based on renewable resources like solar and wind, the intelligent control of distributed energy resources (DERs) including photovoltaic (PV) arrays, controllable loads, energy storage, and plug-in electric vehicles (EVs) will be critical to realizing a power grid that can handle both the variability and unpredictability of renewable energy sources as well as increasing system complexity. Realizing such a decentralized and dynamic infrastructure will require the ability to solve large scale problems in real-time with hundreds of thousands of DERs simultaneously online. Because of the scale of the optimization problem, we use an iterative distributed algorithm previously developed in our group to operate each DER independently and autonomously within this environment. The algorithm is deployed within a framework that allows the microgrid to dynamically adapt to changes in the operating environment. Specifically, we consider a commercial site equipped with on-site PV generation, partially curtailable load, EV charge stations and a battery electric storage unit. The site operates as a small microgrid that can participate in the wholesale market on the power grid. We report results for simulations using real-data that demonstrate the ability of the optimization framework to respond dynamically in real-time to external conditions while maintaining the functional requirements of all DERs.

Index Terms—Distributed energy resources (DERs), distributed optimization, distributed power generation, dynamic pricing, electric vehicles (EVs), energy management, energy storage, microgrids, model predictive control (MPC), photovoltaic (PV) systems, power quality, power system control, smoothing, solar power generation.

I. INTRODUCTION

MOTIVATED by environmental concerns, the need to diversify energy sources, energy autonomy and energy efficiency, the penetration of distributed generation (DG) from renewable resources like solar and wind is rapidly increasing as the trend moves away from large centralized power stations toward more meshed power transmission on the electricity grid. But as penetration of variable generation sources reaches and exceeds the 10%–30% range, matching supply to

load will begin to pose a significant challenge using existing centralized dispatch mechanisms [1]. With these transformations looming in the near-future, the intelligent integration of distributed energy resources (DERs) will become crucial to creating a transaction-based collaborative network that can handle both the variability and unpredictability of renewable energy sources as well as increasing system complexity. While these DERs add system complexity, intelligent control of their power schedules has the potential to serve as a considerable system reliability and stability resource while simultaneously providing a means for greater power system flexibility. This can only be achieved, however, if the ability to solve large scale problems in real-time with hundreds of thousands of devices simultaneously online is integrated into the operation of the power system. Optimization at the distribution level will have to go beyond addressing traditional problems like loss minimization and reactive power compensation and consider the foreseeable transition to a more dynamic power system. DERs can be leveraged to address supply and demand imbalances through demand response (DR) and/or price signals by enabling continuous bidirectional load balancing. DERs acting in coordination could also help reduce or shift demand peaks and improve grid efficiency by displacing the amount of backup generation needed and offsetting the need for spinning reserves and peaking power plants. The dynamic response of a distributed resource located close to the DG source can effectively act as a buffer to match the availability of generation to the draw from online loads. This is critical in low-voltage networks with a high penetration of DG since the absence of buffering through either DR or storage can result in large voltage variations, uncertainty of power flows, and possibly even reversed power flow.

In this paper, we propose a method to realize the shift from a centrally run power grid to a decentralized network that will enable real-time management and scheduling of EVs at a commercial site with PV generation, partially curtailable load and a battery storage unit for backup. While each DER is controlled independently of one another, the capacity constraint at the point of common coupling (PCC) means that in addition to minimizing the cost of power to the microgrid, the controllers must cooperate in such a way as to prevent violation of the physical limitations on the line. Along with demonstrating that DER integration leads to load balancing and rapid response times, we show that the DERs each operate within their constraints. Our method draws upon two key algorithms: using the alternating direction method of multipliers (ADMM) within a model predictive control (MPC)

Manuscript received June 11, 2014; revised December 1, 2014 and February 11, 2015; accepted May 4, 2015. Paper no. TSG-00560-2014.

T. Wang is with the Department of Mechanical Engineering, Stanford University, Palo Alto, CA 94305 USA (e-mail: trudie@stanford.edu).

D. O'Neill is with the Department of Electrical Engineering, Stanford University, Stanford, CA 94305 USA.

H. Kamath is with Electric Power Research Institute, Palo Alto, CA 94306 USA.

Color versions of one or more of the figures in this paper are available online at <http://ieeexplore.ieee.org>.

Digital Object Identifier 10.1109/TSG.2015.2430286

framework, we can distribute the optimization problem among the independent DERs to dynamically and robustly optimize the power flows between them. While there is an abundance of literature that has looked at the response of DERs at various locations on the grid [2]–[4], as well as optimization through MPC for electricity and energy purposes [5]–[7], most work has focused on looking at how the DERs can be centrally and remotely controlled. There has been some recent work done in using distributed dynamic algorithms to optimize the power grid [8]–[11]. However, these approaches make certain assumptions about DER behavior that limit their ability to include new objectives and constraints as well as their adaptability to uncertainty. ADMM allows us to pose the integration of DERs as a completely decentralized control problem whereby each controller only needs to exchange simple messages with its neighbors in the power network in a relatively unconstrained framework. We expand on the ADMM work done previously in our group [12], [13] by looking at how MPC allows us to extend this framework and integrate predictions and state uncertainties as well as constraints for real-DERs into the distributed algorithms dynamically and robustly. The complexity of managing a decentralized network is divided up among all the controllers to make control of the microgrid tractable and reflective of local needs while leveraging local contribution of distribution-level resources.

In our model, each DER only needs to know its own state and historical power profiles in order to determine control actions in the microgrid. In each scenario we explore, we compare avoided costs against potential tradeoffs. We also compare these results to the prescient case for 24 h look ahead horizons to demonstrate that even with simple forecasting models, we are able to operate robustly and very near optimal using ADMM with MPC. This paper models and simulates real-world systems using an integrated dynamic optimization and control framework through which DERs can be scheduled and controlled. Real-measurement data are used to optimize and control the systems. The primary contributions of this research can be summarized as follows. We use MPC with distributed optimization algorithms to carry out dynamic simulations based on real-systems. While DER control and scheduling is a field that is currently rapidly developing and previous work has shown how algorithms can work at a highly theoretical level, this paper model and simulate real-systems in a complete framework to demonstrate that the algorithms used to control and schedule the DERs can work well with actual data in real-world conditions. We also demonstrate that a dynamic controller using MPC can perform near-optimal with limited access to information. Using convex models and simple prediction methods, results come very close to prescient scenarios and this suggests that MPC can be used in embedded controllers to schedule DERs in a way that handles dynamic conditions on the power grid and allows for greater integration of renewable energy resources while maintaining system reliability. DERs scheduled in this way can act as flexible and reliable resources on the grid while operating independently. Increasing responsiveness in the distribution system in this way also has significant implications for reducing costs

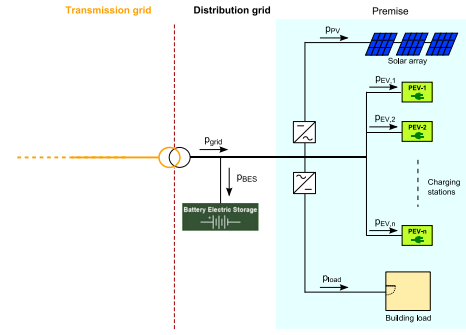


Fig. 1. Schematic representing microgrid with electric load, PV array, BES, and EV charge stations connected to power system. Arrows indicate positive direction of power flow.

associated with system upgrades and procuring more operating reserves. Finally, we demonstrate the synergies that result when a distributed algorithm like ADMM is combined with MPC. Previous work has looked at how distributed methods can be used to schedule DERs or looked at how MPC can be used for dynamic control of DERs, but there has not been an integrated approach looking at how a dynamic MPC framework can be used to execute the schedules determined by the distributed algorithms in a robust and dynamic manner with imperfect and incomplete information. We show that this is not only possible, but it performs very well in cases where DER behavior is coupled due to capacity limited lines and a cooperative approach between the resources is required. This allows various key objectives ranging from integrating renewable generation to DSM to be easily combined.

The remainder of this paper is organized as follows. In Section II, we provide the technical details and the formal mathematical definition of our microgrid model. Section III describes both the MPC framework and the ADMM algorithm used to solve the model. The prediction methods used to make forecasts are also presented. Section V presents a numerical example using wholesale price schedules taken from the California independent system operator (CAISO), PV array and load data taken from a commercial site in Northern California, and EV data from a regional transportation study. The results of our simulations are also given in Section V. Finally, in Section VII we make concluding remarks on our results.

II. MODEL

A. System Dynamics and Constraints

The microgrid modeled and simulated is shown schematically in Fig. 1. Collectively, we refer to the PV array, the charging EVs and the BES unit as the DERs. Each DER and the electric load has an associated power schedule across the simulation time horizon T , with negative power always defined as being power generated and/or flowing out from a point in the microgrid. Note that, we have also treated the connection at the PCC as an effective DER representing the grid with its own objectives and constraints.

The models associated with the microgrid, electric load, and DERs are described in detail below, including the individual objectives and constraints.

1) *Electric Load*: The electric load is represented with a consumption profile, $p_{\text{load}} \in \mathbf{R}^T$. This consumption profile has a diurnal cycle and must be predicted and anticipated using historical load data. We represent the predicted profile as $\hat{p}_{\text{load}} \in \mathbf{R}^T$. When grid-connected or during a contingency situation, the load is curtailable but a minimum time-dependent base load must be met. This is modeled as $\beta \hat{p}_{\text{load}} \leq p_{\text{load}} \leq \hat{p}_{\text{load}}$ where $\beta \in [0, 1]$ is the minimal load fraction that must be met. The value of β will depend on whether the microgrid is operating in a normally functioning power system or if it is facing a contingency situation.

In order to ensure the amount of load that is curtailed on the system is based on the utility function of that load, a curtailment cost is also added

$$\alpha_{\text{load}} \|\hat{p}_{\text{load}} - p_{\text{load}}\|_2^2 \quad (1)$$

where $\alpha_{\text{load}} \geq 0$ is the curtailment penalty parameter.

2) *Photovoltaic Array*: A PV array also follows a diurnal cycle. The power schedule, $p_{\text{PV}} \in \mathbf{R}^T$, is always negative since it only generates power and the peak is offset from the load peak since it occurs when the sun is at its highest. As with the load, the power profile of the PV array is predicted and anticipated using measured historical data. We represent this as \hat{p}_{PV} . The array output will fluctuate with cloud cover and contributes to the power balance on the microgrid but the PV inverter has the option to curtail power if it cannot be pushed back out onto the grid or stored. We model this as $p_{\text{PV}} \leq \hat{p}_{\text{PV}}$.

Since generated power should not be curtailed unnecessarily, a curtailment cost is also included

$$\alpha_{\text{PV}} \|\hat{p}_{\text{PV}} - p_{\text{PV}}\|_2^2 \quad (2)$$

where $\alpha_{\text{PV}} \geq 0$ is the PV curtailment penalty parameter.

3) *Battery Electric Storage*: While the inverter of the PV array can do little more than curtail output, a battery electric storage (BES) unit can store power from the PV array and other DERs and use this to hedge against high prices as well as act as a buffer for requests or unforeseen events on the power grid. Since the BES unit is able to both charge and discharge, its power schedule can be both positive and negative. The rates of charge and discharge are constrained by capacity limits. This is represented as $-D_{\text{BES}}^{\text{max}} \leq p_{\text{BES}} \leq C_{\text{BES}}^{\text{max}}$, where $D_{\text{BES}}^{\text{max}}$ and $C_{\text{BES}}^{\text{max}}$ are the discharging and charging rate limits and $p_{\text{BES}} \in \mathbf{R}^T$ is the BES power schedule.

The dynamics equation governing the state of charge of the BES unit over the time interval $t = 1, \dots, T$ is given by

$$q_{\text{BES}}(t+1) = \eta_{\text{BES}}^q q_{\text{BES}}(t) + \eta_{\text{BES}}^p p_{\text{BES}}(t) \quad (3)$$

where $\eta_{\text{BES}}^q, \eta_{\text{BES}}^p$ lie in the interval $[0, 1]$ and represent the storage and charging efficiencies respectively. The components

of $q_{\text{BES}} \in \mathbf{R}^{T+1}$ are given as some fraction of the nominal capacity and must remain within the capacity limits of the battery. We specify this as $Q_{\text{BES}}^{\text{min}} Q_{\text{BES}}^{\text{cap}} \leq q_{\text{BES}} \leq Q_{\text{BES}}^{\text{max}} Q_{\text{BES}}^{\text{cap}}$ where $Q_{\text{BES}}^{\text{min}}, Q_{\text{BES}}^{\text{max}}$ lies in the interval $[0, 1]$ and $Q_{\text{BES}}^{\text{cap}}$ represents the nominal rating of the unit. The BES unit can also have associated costs, including a cycling cost to penalize excessive charge-discharge cycles

$$\alpha_{\text{cyc}} \sum_{t=1}^{T-1} |p_{\text{BES}}(t+1) - p_{\text{BES}}(t)| \quad (4)$$

where $\alpha_{\text{cyc}} \geq 0$ is the cycling penalty parameter.

A terminal constraint can additionally be added to the BES unit to ensure that the storage system is not depleted at the end of the time horizon, with a common choice of q_{final} being $0.5Q_{\text{cap}}$ or the initial charge state of the battery.

4) *Electric Vehicle*: An EV is a flexible load with storage capabilities that allows charging to be deferred as well as discharging when economical. It differs from the BES unit in that it has additional constraints in both availability and required charge capacity. The microgrid has N_{EV} EVs onsite and each EV has an associated charging schedule $p_{\text{EV},i} \in \mathbf{R}^T$ and charge state $q_{\text{EV},i} \in \mathbf{R}^{T+1}$ where $i = 1, \dots, N_{\text{EV}}$. When the vehicle is not plugged in, $p_{\text{EV},i}(t) = 0$ and $t = T_{\text{dep}}(i) + 1, \dots, T$. The EVs are also associated with four stochastic variables, namely the arrival time, departure time, initial charge state, and desired charge state. We write this as a four-component vector $\theta_{\text{EV},i} = [T_{\text{arr}}, T_{\text{dep}}, q_{\text{init}}, q_{\text{des}}]_{\text{EV},i}$. For each EV, the components of $\theta_{\text{EV},i}$ need to be predicted using probability distributions based on historical data prior to the arrival time. After arrival, the vector is completely defined.

The vehicles also have charge constraints $-C_{\text{EV},i}^{\text{max}} \leq p_{\text{EV},i} \leq C_{\text{EV},i}^{\text{max}}$ where $C_{\text{EV},i}^{\text{max}}$ is the maximum charge/discharge rate of the i th EV

$$q_{\text{EV},i}(t+1) = \eta_{\text{EV},i}^q q_{\text{EV},i}(t) + \eta_{\text{EV},i}^p p_{\text{EV},i}(t) \quad (5)$$

where $\eta_{\text{EV},i}^q, \eta_{\text{EV},i}^p$ lie in the interval $[0, 1]$ and are the storage and charging efficiencies respectively. $q_{\text{EV},i}$ is additionally constrained by the capacity of the battery. This is specified as $Q_{\text{EV},i}^{\text{min}} Q_{\text{EV},i}^{\text{cap}} \leq q_{\text{EV},i}(t) \leq Q_{\text{EV},i}^{\text{max}} Q_{\text{EV},i}^{\text{cap}}$ where $Q_{\text{EV},i}^{\text{min}}, Q_{\text{EV},i}^{\text{max}}$ lie between $[0, 1]$ and are the minimum and maximum charge levels of the batteries. $Q_{\text{EV},i}^{\text{cap}}$ is the nominal rating of the i th EV battery.

The desired state of charge for each vehicle $q_{\text{des},i}$ is also used to represent the utility of each vehicle through the constraint

$$q_{\text{EV},i}(T_{\text{dep},i}) \leq \alpha_{\text{des},i} q_{\text{des},i} \quad (6)$$

where a higher $q_{\text{des},i}$ indicates a greater demand for power and $\alpha_{\text{des},i}$ represents the vehicle owner's flexibility for not meeting the desired departure state. The utility functions of each vehicle can be learned and/or specified, enabling vehicle owners to assign values to desired charging services and then scheduling their vehicles to maximize net benefits based on these assignments. While methods of determining the utility

functions of individual vehicles can readily be incorporated into our model, for simplicity we assume that the utility functions have already been determined and focus on showing that the distributed algorithms can handle varying utility functions for the vehicles simultaneously.

A penalty for excessive cycling of the vehicle battery can also be included for each vehicle

$$\alpha_{cyc,i} \sum_{t=1}^{T-1} |p_{EV,i}(t+1) - p_{EV,i}(t)| \quad (7)$$

where $\alpha_{cyc,i} \geq 0$ is a penalty parameter that weights the excessive cycling cost against the utility function of the vehicle.

5) *Grid Connection*: The microgrid is connected to the power grid at the PCC where power is stepped up or down in voltage and the wholesale rate for power is applied. From the perspective of the power controller that sits behind the meter, this connection acts as a power limiter that caps the amount of power that can be transmitted over the line. We model this as

$$|p_{grid}| \leq P_{PCC} \quad (8)$$

where $p_{grid} \in \mathbf{R}^T$ is the power schedule at the PCC and P_{PCC} is the power limit at the PCC. p_{grid} can take on both positive and negative values depending on whether the power is being taken from the grid or put back onto the grid. At the PCC, the cost function minimizes energy cost as well as the cost of regulation

$$\sum_{t=1}^T c(t)p_{grid}(t) + f_{smooth}(p_{grid}(t)). \quad (9)$$

In the first term, c is the real-time wholesale price schedule for power. The microgrid receives this price schedule from the independent system operator (ISO) and uses it in the first term to determine what power profile will minimize the cost of power drawn from the grid over the price time horizon. When the term is negative, the microgrid is selling power to the power grid and making a profit. While there are many methods to achieve energy arbitrage and shift demand at the distribution level, the most practical and effective technique is often to simply use real-time wholesale pricing since they are best positioned to allow both consumers and providers to participate and benefit from power transactions as the power grid develops into a more dynamic and responsive system [14]. The second term is the cost associated with the smoothness of the output at the PCC. It ensures a smooth power profile that does not sharply increase or decrease due to PV output or sudden load changes in the microgrid. This measure of power quality can in some cases be remunerated for by the ISO and in other cases is required in order to connect to the power grid and avoid penalties. For this term, we consider a weighted sum of three different measures of smoothness to account for the maximum range, slope, and curvature of the power output. This minimizes the variation in magnitude and rate of change of the output to produce a more consistent and smoother power profile.

We represent this term as

$$\begin{aligned} f_{smooth}(p_{grid}(t)) = & \alpha_{range} \left(\max_t p_{grid}(t) - \min_t p_{grid}(t) \right) \\ & + \alpha_{diff} \sum_{t=1}^{T-1} |p_{grid}(t+1) - p_{grid}(t)| \\ & + \alpha_{curv} \sum_{t=1}^{T-2} (p_{grid}(t) - 2p_{grid}(t+1) \\ & + p_{grid}(t+2))^2 \end{aligned} \quad (10)$$

where α_{range} , α_{diff} , and α_{curv} are the penalty parameters for tuning the range, slope, and curvature terms, respectively.

B. Objective

Because our objectives are distinct and separable, we can consider a cost function that is equal to the sum of the individual objectives. This objective is minimized subject to the power flow balance constraint

$$\begin{aligned} & \text{minimize} \quad \sum_{i=1}^N f_i(p_i) \\ & \text{subject to} \quad \sum_{i=1}^N p_i = 0 \end{aligned} \quad (11)$$

where $N = 4 + N_{EV}$ is the total number of independent controllers onsite (i.e., load, PV, BES, PCC, and EVs) and f_i represents the objective and constraints of each controller. We set $f_i(p_i) = \infty$ to represent infeasibility of the power schedule of the i th controller. When $f_i(p_i) < \infty$ for $i = 1, \dots, N$ and the constraint ensuring power balance is satisfied, the solution is feasible and p_i represents a realizable schedule with $f_i(p_i)$ being the associated cost of that schedule. It is important to note that only the controller at the PCC is provided with the external price schedule and it determines its own power profile. As will be explained in Section III, even though it is the interface between the power grid and the other DERs, it does not need to know anything about them or control their behavior. The power balance constraint is a physical constraint that ensures all controllers in the microgrid coordinate to achieve a feasible solution.

C. Control Policy

The control policy for each DER in our microgrid selects the control variables based on information available at the current time. Known information includes DER parameters, grid line limits and conditions at the PCC, and measured states of the DERs and loads. This information along with external wholesale prices and estimates of unknown quantities are then used to calculate and minimize the total cost. Through this optimization process, the control policy determines the power schedules of each controller onsite.

III. METHOD

In this section, we briefly describe the algorithms we use to control and optimize the DERs. We begin by describing the

Algorithm 1 Iterative Optimization Using MPC

```

Initialize charge states  $q_{\text{BES}}(1), q_{\text{EV},i}(1) \quad \forall i = 1, \dots, n$ 
for  $t = 1 \rightarrow T$  do
    Predict  $\hat{p}_{\text{PV}}$  and  $\hat{p}_{\text{load}}$  using updated historical power
    profiles available at time  $t$ ;
    Update EV parameters  $\hat{\theta}_{\text{EV}}$  using charge data as well as
    arrival and departure times available at time  $t$ ;
    Solve ADMM problem over MPC time horizon
     $[t, t + T_{\text{MPC}}]$ ;
     $q_{\text{BES}}(t + 1) \leftarrow \hat{q}_{\text{BES}}(t + 1)$ ;
     $q_{\text{EV},i}(t + 1) \leftarrow \hat{q}_{\text{EV},i}(t + 1) \quad \forall i = 1, \dots, n$ ;
end for

```

MPC framework that adaptively controls the DERs. We then describe how we can solve the optimization problem described in Section II using ADMM equations to distribute the computational effort. The ADMM solution is used by MPC to execute control actions at each time step. Finally, we describe the algorithms we use to make predictions of unknown variables that are passed on as inputs to the optimization problem.

A. Model Predictive Control

MPC is a control policy that can be used to dynamically control each DER independently. Its ability to handle uncertainty and dynamics in real-time allows it to operate robustly in a changing environment. Within the MPC framework, the optimization problem is solved dynamically at each time step using the decentralized ADMM algorithm to determine an action policy for each controller in the microgrid and enable scheduling of the controllable DERs over a finite time horizon.

To implement MPC, we first solve the optimization problem at the current time step t using ADMM to determine a series of conditional power schedules for each controllable DER over a fixed time horizon extending T_{MPC} steps into the future. Since ADMM convergence is on the order of milliseconds and microseconds [15], [16], actions and schedules are determined well before the next time step in MPC at which point the microgrid responds to the updated state of the power system (generally on the order of minutes). Each controller then executes the first step of its schedule and idles until the next time step at which point the entire optimization process is repeated in order to incorporate changes in operating environment, as well as new state measurements and external information that may have subsequently become available. This iterative process ensures that the ADMM solution is robust to measurement errors, missing information, and inaccurate forecasts, ensuring that the control policy dynamically adjusts and is self-correcting as new information arrives and changes in the operating environment occur. MPC is thus well suited for use with ADMM in dynamic operation of a microgrid, especially when there is uncertainty in the system [15]. Algorithm 1 outlines the iterative process used by the MPC method.

In order to avoid oscillations between MPC iterations, we have also added a regularization term to each objective function f_i which we specify as $f_i^{\text{prev}} = \alpha^{\text{prev}} \|\hat{p}_i - \hat{p}_i^{\text{prev}}\|_2^2$,

where \hat{p}_i^{prev} is the solution for the previous iteration and α^{prev} is the damping weight for oscillations between iterations. This prevents the solution at the current time step from diverging too far from the previous time step and ensures that smoothness across the MPC prediction horizon does not come at a cost to smoothness between the current time step and previous time steps.

B. Alternating Direction Method of Multipliers

In ADMM, we solve the optimization problem specified in (11) using the methods developed in [13] and [12]. Each controller in the microgrid effectively participates in an internal market with a price adjustment process that is used to attain general market equilibrium. The internal price of power is increased or decreased depending on whether there is an excess demand or excess supply respectively. This internal price will naturally reflect the external price at the PCC but is not necessarily equivalent since it also reflects the individual interests of the independent DER controllers within the microgrid. The complete derivation of ADMM for the exchange problem can be found in [12] and [13]. We summarize the main equations from the derivation and ask the reader to refer to [12], [13] for more details. The ADMM algorithm can be written as

$$p_i^{k+1} := \underset{p_i}{\operatorname{argmin}} \left(f_i(p_i) + (\rho/2) \|p_i - p_i^k + \bar{p} + u^k\|_2^2 \right) \quad (12)$$

$$u^{k+1} := u^k + \bar{p}^{k+1} \quad (13)$$

where $\rho > 0$ is the penalty parameter and $\bar{p} = (1/N) \sum_{i=1}^N p_i$ represents the mean of the p_i variables.

In each iteration of the p -update in step (12), ADMM augments its own local objective function f_i with a simple quadratic regularization term. The linear parts of the quadratic terms containing the iterative target value are then updated, pulling the variables toward an optimal value and allowing them to converge. This proximal operator contains the scaled price u^k and can be interpreted as a penalty for p_i^{k+1} deviating from p_i^k projected onto the feasible set, helping pull the variables p_i toward schedules that enable power balancing while still attempting to minimize each local objective. In other words, it represents each controller's commitment to help reach market equilibrium so that as the power profiles are adjusted and the system converges, the effect of the regularization term vanishes. External price signals can still be used as an input to help the power grid achieve system-wide objectives but each local controller exchanges messages containing the internal price signal in order to align locally optimized operating policies with the goals that benefit the entire system. These goals can range from transmission and operation costs to environmental costs to minimizing capital and fuel expenditures. At convergence, the internal price resulting from running ADMM represents the optimal equilibrium price that occurs when the objectives are mutually optimized.

Since each controller only handles its own objectives and constraints, the p -update can be carried out independently in parallel by all the controllers in the microgrid. This means that the optimization problem with at least as many variables as the

number of DERs and loads multiplied by the length of the time horizon is reduced to small local optimization problems with only a few variables for each controller to manage, including local power flows and internal states. The controllers pass their updated power schedules, p_i^{k+1} , to a collector (possibly co-located at the PCC) in the u -update (13) which in turn simply gathers the variables and computes the new average power imbalance, \bar{p}^{k+1} , in order to update the scaled price u^{k+1} . The computed values are then broadcasted back to the controllers to readjust the proximal operator. In this way, the collection stage projects the power schedules back to feasibility and helps push the system toward equilibrium by adjusting the price up or down depending on whether there is net power demand or generation in the system. The iterative ADMM algorithm converges by alternating between the controllers and the collector with synchronization (necessary for real-time pricing in any event) being the only coordination that is required between the controllers. Since optimization is independent and allows for autonomous operation with minimal coordination, this bottom-up control approach through ADMM makes it feasible to connect large numbers of these distributed systems to the grid without requiring the implementation of complex top-down control systems. This paradigm shift allows for a new way to think of operating the grid since it can allow for both efficient energy trade and active flexible control of power flows at the controller level.

When implementing ADMM, selecting the correct penalty parameter ρ is critically important for convergence rates. The optimal value of ρ will greatly depend on the scheduling problem. While there are heuristic methods to help determine the value of ρ , in many cases it will perform just as well with a fixed value found using a binary search method. Since we are using a scaled form of ADMM, the scaled dual variable $u^k = (1/\rho)y^k$ must also be rescaled after updating ρ . This means that if ρ is halved, u^k should be doubled before computing the ADMM updates.

IV. PREDICTIONS

To implement MPC and provide inputs for the optimization problem, estimates of unknown variables are required at each time step over the finite time horizon. These estimates can be based on historical data, stochastic models, forecasts, and pricing information. The flexibility of the MPC framework means that it is not tied to any specific forecasting method and can incorporate a range of techniques depending on what information can be accessed. Perfect predictions or a formal statistical model to represent uncertainty are also not required for the method to perform robustly and predictions that capture general trends are sufficient since MPC recalculates power schedules at each time step after executing the first step of the previously determined schedule, dynamically adjusting and self-correcting for any past errors or missing information [15], [17].

A. Power Profiles

Within the microgrid, predictions are required for the output of the PV array and the electric load. While many methods

have been used to predict energy profiles on the power grid, ranging from multiple regression to expert systems [18], [19] and total load over a large region can be predicted up to 1% accuracy, predicting generation locally from intermittent renewable resources poses a greater challenge due to nuances that require detailed knowledge of the system environment and geographic diversification cannot smooth out [20]. Since our objective is to only capture general trends and the DERs just needs to forecast their own future power profiles in each time period, we require only local measurements of historical output to get adequate predictions.

To predict PV output, we use the prediction model defined in [21]. We first assume that the historical PV output data $p_{PV}^{\text{hist}} \in \mathbf{R}_{\text{hist}}^T$ has general periodicity over a 24 h period, where T_{hist} is the historical time horizon. This is a good assumption over a period of a few days where the seasonal variation is insignificant since the solar insolation at any geographical location and given time is well determined. Deviations from the expected PV array output are due to weather conditions like cloud cover that result mostly in drops in output with occasional over-irradiance due to cloud enhancement effects. This leads up to propose an asymmetric least squares fit of the available historical PV output data to provide a periodic baseline that is weighted toward the outer envelope of the observed data. To generate the PV output prediction, we first determine the historical baseline $\hat{p}_{PV}^{\text{hist}}$ by solving an approximation problem with a smoothing regularization term and a periodicity constraint

$$\begin{aligned} \underset{\hat{p}_{PV}^{\text{hist}}}{\text{minimize}} \quad & \frac{1}{T} \sum_{\tau=t-T_{\text{hist}}+1}^{t-1} \left(\left(\hat{p}_{PV}^{\text{hist}}(\tau) - p_{PV}^{\text{hist}}(\tau) \right)_+^2 \right. \\ & \left. + \gamma_{\text{asym}} \left(\hat{p}_{PV}^{\text{hist}}(\tau) - p_{PV}^{\text{hist}}(\tau) \right)_-^2 \right. \\ & \left. + \gamma_{\text{curv}} \left(\hat{p}_{PV}^{\text{hist}}(\tau-1) - 2\hat{p}_{PV}^{\text{hist}}(\tau) + \hat{p}_{PV}^{\text{hist}}(\tau+1) \right)^2 \right) \\ \text{subject to} \quad & \hat{p}_{PV}^{\text{hist}}(\tau) = \hat{p}_{PV}^{\text{hist}}(\tau + T_{\text{period}}) \\ & \tau = t - T_{\text{hist}} + 1, \dots, t - 1 \end{aligned} \quad (14)$$

where $(z)_+ = \max(0, z)$ and $(z)_- = \min(0, z)$. γ_{asym} and γ_{curv} represent the weights for the asymmetric and curvature terms respectively and T_{hist} is the amount of time over which p_{PV}^{hist} occurs. The first and second term of the objective function represent the positive and negative deviation of the predicted curve from the actual data and the third term smooths the curvature in the predicted curve. The first term is weighted more heavily to push the predicted curve toward the outer envelope of the fluctuating data. The constraint ensures periodicity across $T_{\text{period}} = 24$ h. Solving this problem de-noises the data to reconstruct a smooth baseline profile [22]. The objective function is a weighted sum of squared convex terms and forms a regularized convex problem which tradeoffs an asymmetric least-squares fit against the mean-square curvature of the data. The baseline prediction for the MPC horizon is then defined as $\hat{p}_{PV} = \hat{p}_{PV}^{\text{hist}}(t - T_{\text{period}}, \dots, t + T - T_{\text{period}})$.

Once we determine this baseline prediction, we correct for transient weather phenomena by adjusting the baseline using an error fit with a linear model applied to the

residual $r = \hat{p}_{PV}^{\text{hist}} - p_{PV}^{\text{hist}}$. We can rewrite this concisely in matrix form

$$\|e\|_2^2 = \|Ma - b\|_2^2 \quad (15)$$

where

$$b = \begin{bmatrix} r(n+1) \\ r(n+2) \\ \vdots \\ r(T_{\text{hist}}) \end{bmatrix}$$

$$M = \begin{bmatrix} r(n) & r(n-1) & \vdots & r(1) \\ r(n+1) & r(n) & \vdots & r(2) \\ \vdots & \vdots & \vdots & \vdots \\ r(T_{\text{hist}}-1) & r(T_{\text{hist}}-2) & \vdots & r(T_{\text{hist}}-n) \end{bmatrix}.$$

The predicted residual corrections across the MPC horizon are then decreased by a factor λ at each future time step, where $0 < \lambda < 1$. This reduces the magnitude of the correction over the MPC horizon moving forward in time so that the prediction reverts back to the baseline.

We employ a similar approach for the electric load using the historical load profile $p_{\text{load}}^{\text{hist}} \in \mathbf{R}_{\text{hist}}^T$. The only difference between the PV and load profiles is that with the load, we weight the first and second term of the objective function equally since we expect the positive and negative deviation of the predicted curve from the actual data to be similar. This prediction method is simple to implement using available historical data and requires very little computational effort during real-time implementation. While the flexibility of our prediction method means that it is trivial to incorporate additional data by including a weighted term to the asymmetric least squares objective.

B. EV Parameters

In order to predict the stochastic variables in $\theta_{EV,i}$ for $i = 1, \dots, n$, we first consider whether or not a given EV has arrived. In the case where an EV has arrived, we assume $\theta_{EV,i}$ is known. If a vehicle has not arrived, we need to predict $\theta_{EV,i}$ using available data. Ideally, there would be enough data to form approximately stationary prior probability distributions for each of the variables in $\theta_{EV,i}$. In practice, there will initially be insufficient data to make accurate predictions for each vehicle. As time progresses, however, accumulation of data will lead to more stationary distributions and predictions will become increasingly accurate. In fact, for this reason it is common practice to ignore some number of samples at the beginning before the stationary distribution to be reached. However, for MPC even a general forecast can produce good results as our results will later show.

To predict T_{arr} and T_{dep} , we use maximum likelihood estimates from stationary probability distributions. While we could construct conditional probability distributions that are time dependent using Markov chains that adjust the stationary prior probability distribution, we found that this method added insignificant or no benefit since MPC already corrects

for prediction error and hence already performs near optimal with rough predictions. The fact that the stationary probability distributions are fairly time independent after enough data has been acquired means that this prediction method performs satisfactorily and is preferred for its minimal computational requirements.

Since there is no reason to assume the state of charge variables are strongly and independently correlated with the time variables, we similarly use stationary distributions to determine arrival and desired departure charge states. For q_{init} , this means computing the maximum likelihood once daily for the vehicles that have not yet arrived. To determine the desired charge state q_{des} , we employ a more conservative approach to determine how much charge the vehicle batteries have to at least have at departure time. Instead of a maximum likelihood, we consider the highest charge state in the distribution since it is assumed that the driver will want to ensure there is enough charge to face the majority of contingency situations. Although this is overly conservative in the case of a plugin hybrid EV which has the option to use gasoline as backup, gasoline prices will inevitably continue to trend upward and running solely on the electric battery will become increasingly desirable so that the assumptions made serve as a good first approximation for setting a desired charge state. From a carbon standpoint, ensuring the maximum number of electric miles will also have the best possible societal benefit. As more data for each vehicle is accumulated, the model can easily be adapted to the needs of individual vehicle owners in real-time. After a vehicle arrives, the charge states along with the times of arrival and departure are added to the data and the predictions are updated the next day.

V. NUMERICAL EXAMPLE

Simulations are run using real-load and generation data taken from May 18–25, 2013. For the simulation period, we also use day-ahead hourly wholesale price data published by the CAISO [23]. In each scenario we simulated, we selected an MPC time horizon of $T = 96$. This corresponds to 15 min intervals over a 24 h period and is a typical horizon and time step for schedule updates. The time step $\tau = 1$ corresponds to midnight.

The microgrid is connected to the distribution system through a bidirectional meter which has access to the real-time wholesale prices. The connection also has a physical transfer constraint $P_{\text{PCC}} = 200$ kW. The power profile for the electric load is taken from measurements at a typical commercial site and the PV output is taken from the output of a rooftop PV array, both geographically co-located in Northern California. We size the array to 1200 kW and scale the output accordingly so that it is able to meet all of the local energy demands of the load over a diurnal cycle when islanded. This data is incorporated into the model both as simulation data and as historical data to help make predictions and schedule the DERs. As time proceeds, the simulation data is added onto the historical data incrementally at each time step and used to update the predictions. The predictions are made using five days of historical data to predict the next 24 h of generation. While it

TABLE I
BES PARAMETERS

Parameter	Value
$C_{BES}^{\max} = D_{BES}^{\max}$	500kW
$\eta_{BES,c} = \eta_{BES,d}$	0.85
$\eta_{BES,q}$	0.90
Q_{BES}^{\min}	0.20
Q_{BES}^{\max}	0.90
Q_{BES}^{cap}	3000kWh

may seem that P_{PCC} is overly limiting, the aim is to demonstrate that the microgrid can run flexibly and reliably on a grid of limited capacity using dynamic algorithms to handle the coupling constraints. The on-site BES unit is sized to provide sufficient capacity to arbitrage energy for islanding situations while maintaining at least 50% baseload [24], [25]. All BES parameters are provided in Table I. Within the microgrid, a fleet of 20 EVs is available and capable of level 2 charging at 7.2 kW without requiring a dedicated circuit [26]. Battery efficiency values $\eta_{EV,i}^q, \eta_{EV,i}^p$ are both set at 90% [27]. The battery capacity for each vehicle is selected based on driver need. In other words, as an appropriate first approximation it is assumed that vehicles with longer commute distances will have vehicle owners who desire larger batteries. Using individual vehicle data taken over several hundred days in a study conducted by EPRI [28], we consider the longest trip distance and use a $2\times$ buffer along with a typical mileage conversion rate of 0.311 kWh/mile [29]. The minimum and maximum charge states of the batteries are selected to be 30% and 90%, respectively, to avoid deep cycling of the battery [27]. The arrival times T_{arr} and departure times T_{dep} for each vehicle are chosen from distributions constructed using the vehicle data. The value of q_{init} is determined using a Monte Carlo method to select from the distribution of initial charge states. For the desired charge state q_{des} , we use the conservative approach described in Section IV.

The cycling penalty parameters as well as other penalty parameters and utility function weights were assigned unitary value since they are dependent on actual user preferences which we did not have access to. For an initial proof of concept, this does not affect either the applicability or validity of the results presented as there is no loss of generality. While each of the weights will be system specific and dependent on the objectives and constraints of each model, the parameters we use can provide a good initial starting point for a range of systems. Each specific system will then require some initial tuning to ensure performance in real-time meets particular requirements and objectives. Because the cost functions for each DER were relatively well scaled and of similar magnitudes, selecting the weights to be approximately equal for optimal ADMM convergence rates also made practical sense. The value of ρ is then selected using a binary search method to minimize the total cost to the system.

VI. RESULTS

The results of our simulations over a three-day period are provided below in Table II. In addition to carrying out the

simulation using the ADMM method to distribute the optimization calculations among the controllers, we simulate a case with a microgrid carrying out the same calculations through centralized optimization as well as a centralized case with prescient knowledge in order to provide a benchmark for how ADMM with MPC performs even with simple prediction methods. In the prescient case, instead of using predictions we assume PV and load schedules as well as EV parameters are fully known over the MPC horizon. For each scenario simulated, we calculate the cost of energy at the PCC as well as for each DER. We also determine the ramping cost at the PCC represented by (10), the power curtailed by the PV array and load, and the total energy shortfall when charging the EVs to their desired departure state of charge.

As the table shows, ADMM performs similarly to the centralized method and both come very close to the performance of the centralized prescient method. Comparing the ADMM and the centralized case, there is less than a 1.5% difference between the total system costs. Contrasting both of them against the ideal centralized prescient case, there is less than a 3.3% difference between the total system costs. Plots of the ADMM and the centralized cases for the simulation period are provided below. The net power profile of the microgrid at the PCC is shown first in Fig. 2, plotted against the net power profile that results from PV and load without any optimization to compare the performance of the microgrid against the base case. Note that, we have moved p_{grid} to the other side of the power balance constraint in the scheduling problem in order to maintain the convention that consumed power is positive and generated power is negative. This plot is followed by plots of the PV array output in Fig. 3 and the load power profile in Fig. 4 after curtailing. The power profile and state of charge of the BES unit and the EVs are provided in Figs. 5 and 6, respectively. The state of charge in the latter case is plotted as a percentage of the total capacity of all the vehicles beginning each day at the time when the first vehicle arrives and ending at when the last vehicle departs. From the plots comparing ADMM with the centralized case, it can be seen that the results are very similar and this corroborates the quantitative results from Table II. Since the capacity limit of the line is binding, the DERs use their resources to ensure the microgrid can still operate within these limits, absorbing excess generation from the PV array to sustain the load when PV generation drops off. This can be seen in Fig. 2, where some smoothing in the power profile is noted with fewer intermittent spikes due to either load or generation but the PCC profile is shaped primarily by the capacity limit. The generated output is relatively flat throughout the peak price hours before dropping off each evening as the price begins to decrease. There is then a constant load for the remaining hours until the PV output begins to increase again along with the price. The PV output is initially insufficient to meet the load which begins to go up earlier so both the BES unit and EVs discharge slightly to help with the load in the face of increasing prices. There is still some flexibility with the storage unit and EVs after the PV output falls off each day, allowing the DERs to use their capacity for energy arbitrage and respond to the still high prices by shifting the power generated by the PV array from

TABLE II
COST METRICS FOR SIMULATED SCENARIOS

Method	External cost [\$]	Smoothing cost [kW]	PV curtailed [kWh]	Load curtailed [kWh]	EV shortfall [kWh]
centralized (prescient)	-1682.59	14.99	902.63	122.05	0
centralized	-1680.62	16.36	918.48	114.94	0
ADMM decentralized	-1674.74	16.67	919.64	116.65	0

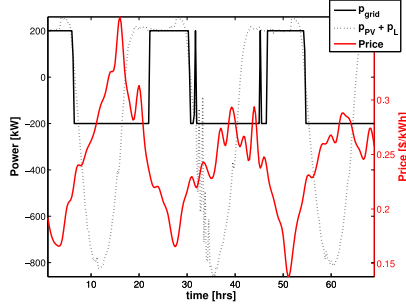


Fig. 2. Power profile of microgrid at PCC over the simulation time horizon using ADMM. The output is plotted against price and the unoptimized net power profile of the PV array and load.

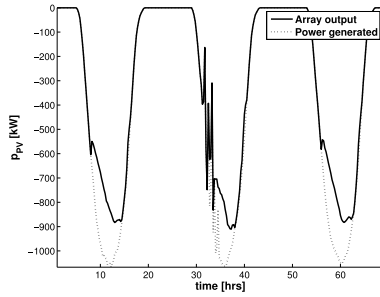


Fig. 3. Power output of the PV array over the simulation time horizon using ADMM. The output is plotted against the actual power produced by the array before curtailing.

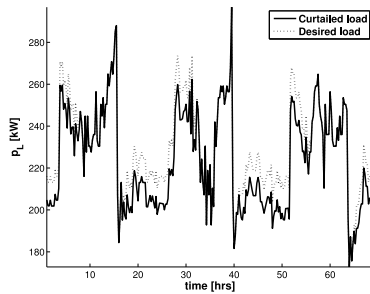


Fig. 4. Power profile of the curtailed building load over the simulation time horizon using ADMM. The output is plotted against the desired power prior to curtailing.

its peak time at 12 to 5 P.M. when the peak price occurs. This completely offsets the load at the peak price time in order to increase net profit.

From Fig. 3, there is evidence of some curtailing of generated PV power during peak generation hours when there is not enough capacity both on-site and through the grid connection to absorb that energy. The power is curtailed around the peak generation hour when the price for power is still relatively low. In Fig. 4, a small amount of load curtailment

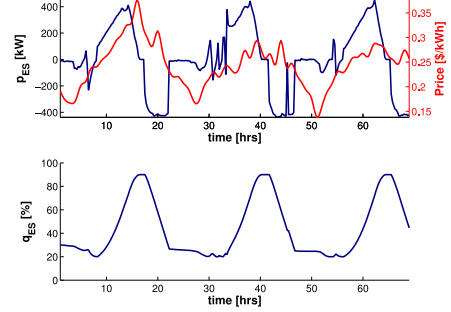


Fig. 5. Top plot shows the power profile of the BES unit plotted against price using ADMM. In the bottom plot, the state of charge of the BES unit is plotted as a percentage of the total battery capacity.

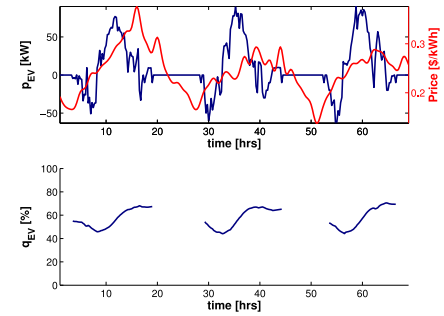


Fig. 6. Top plot shows the net power profile of the EVs plotted against price using ADMM. In the bottom plot, the state of charge of the EVs is plotted as a percentage of the total vehicle battery capacity.

also occurs during the evening hours when no solar energy is being generated and the line capacity has been reached in terms of how much power can be imported. In both cases, however, the curtailing is not substantial since both the BES unit and the EVs use their storage capabilities to minimize these effects. The BES unit undergoes a deep discharge daily as shown in Fig. 5 during peak prices when there is no PV output and charges again to full capacity when prices drop and PV output increases. The EVs behave similarly in Fig. 6, with the aggregate of vehicles charging as the price generally decreases and discharge excess capacity when the price generally increases. The reason for the smooth charging profile of the vehicles is that while individual charging can be more intermittent when responding to real-time pricing and each vehicle has arrival and departure constraints that limit their flexibility, the aggregate effect of a diverse population can actually produce a smoother net power profile with some degree of coordination without having to impose a smoothing constraint or centralized top-down control [30], [31]. This is helped by the fact that when optimizing power schedules through ADMM, the line limit forces each EV to account

for the implications of simultaneously drawing power at start up when voltages are low and this presents a natural way to reintroduce diversity by automatically giving priority to the vehicles most willing to accept the high costs without any subjective ordering. Hence, the vehicles can be viewed within the microgrid as one single entity with predictable emergent characteristics that can be incentivized to charge in a way which helps to meet system wide objectives even though each vehicle is controlled independently in a decentralized fashion and does not need to over-cycle significantly on an individual basis. This is a notable finding since there is currently a large amount of concern over how the proliferation of EVs may tax an already strained grid with their relatively substantial charging requirements at the distribution level [32]. Both the predictability of the net power profile and its flexibility to charge at specific hours shows in fact that the EVs can play a very useful role in DR even when control is distributed to each vehicle. Responding in this way through the demand side can provide a potentially more economical way to automate and dynamically respond to changing conditions on the power grid compared to transformers, load tap changers, and capacitor banks. Also, note that while only the controller at the PCC is aware of the wholesale price schedule and the grid connection limit, all DERs on-site operating independently can help shape P_{grid} through ADMM and ensure the limiting constraints are not violated.

While the primary aim of the simulations was to demonstrate the ability of dynamic distributed algorithms to schedule DERs cooperating when faced with a coupling constraint, this example also shows that a microgrid using such algorithms can produce very reliable and consistent power profiles when provided with the right incentives even if its only generation source is intermittent solar. This means that power can be provided with higher power quality and a higher load factor in addition to responding to real-time prices. Such services are critical in a more distributed and decentralized grid where contingency events can lead to catastrophic circumstances as the grid becomes increasingly less foreseeable and controllable. The ability to shape p_{grid} using the capacities and demands of each DER benefits both the system operator and the microgrid since it means the system can be run more efficiently at a lower cost and the impacts of tiered pricing can also be avoided.

A. Computation Times

The simulation is carried out using code generation for convex optimization [16] to solve the optimization at each time step. Using open-source solvers, it runs in a MATLAB environment and is hence ideal for rapid code development and deployment. Since MPC uses the first step of the previous solution to provide a warm start for ADMM in the next iteration, the optimization problem at each MPC iteration can be solved on an Intel Xeon 3.0 GHz dual core processor in approximately 1–4 s for each DER. The predictions at each time step are similarly solved and require an additional 1–4 s. This means that the amount of time required at each time step will be significantly less than the amount of time

lapsed between time steps, making real-time dynamic solutions entirely feasible. While this demonstrates that our methods are suitable for real-time implementation, it should be noted that we were carrying out simulations using MATLABs interpreted language as a proof of concept before actual implementation using embedded compiled code. Hence, the times reported are conservative approximations only and significantly better performance times can be attained in the milliseconds time frame [13].

VII. CONCLUSION

We have developed a framework using MPC and ADMM to control and optimize a microgrid with PV, curtailable load, EV charge stations, and a stationary BES unit. This paper extends [13] that focused on using ADMM to solve the power scheduling problem. When used with MPC, the algorithms distribute and decentralize the optimization problem and require only local information and simple prediction methods to work while retaining the ability to incorporate any additionally available information into the objectives and constraints of both the entire system and individual DERs as time progresses. By distributing control through ADMM, the problem of managing the microgrid is made more tractable by enabling a cooperative approach between the resources while still respecting coupling constraints due to capacity limited lines. MPC ensures the executed power schedules adapt and keep the system both flexible and resilient when there is imperfect information or sudden unexpected changes to the system. Using data taken from the EPRI campus in Northern California and transportation data taken from a national survey, we simulated and compared the performance of the algorithms. Our simulations demonstrate that each device is able to retain functionality while allowing the microgrid to respond to external price signals and physical power line limits as well as contingency events. With minimal information sharing between devices, we can obtain performance results that are comparable to those obtained when the optimization problem is solved centrally with prescient knowledge.

ACKNOWLEDGMENT

The authors would like to thank E. Chu and M. Kraning for extensive discussion on the problem formulation and prediction methods, and S. Boyd for his advising and guidance on the problem formulation and prediction methods.

REFERENCES

- [1] P. Denholm, E. Ela, B. Kirby, and M. Milligan, "The role of energy storage with renewable electricity generation," Nat. Renew. Energy Lab., Golden, CO, USA, Tech. Rep. TP-6A2-47187, 2010.
- [2] L. Ying and M. Trayer, "Automated residential demand response: Algorithmic implications of pricing models," in *Proc. IEEE Int. Conf. Consum. Electron. (ICCE)*, Las Vegas, NV, USA, 2012, pp. 626–629.
- [3] N. Li, L. J. Chen, and S. H. Low, "Optimal demand response based on utility maximization in power networks," in *Proc. IEEE Power Energy Soc. Gen. Meeting*, San Diego, CA, USA, 2011, pp. 1–8.
- [4] M. A. A. Pedrasa, T. D. Spooner, and I. F. MacGill, "Coordinated scheduling of residential distributed energy resources to optimize smart home energy services," *IEEE Trans. Smart Grid*, vol. 1, no. 2, pp. 134–143, Sep. 2010.

- [5] H. Hindi, D. Greene, and C. Laventall, "Coordinating regulation and demand response in electric power grids using multirate model predictive control," in *Proc. IEEE PES Innov. Smart Grid Technol.*, Anaheim, CA, USA, 2011, pp. 1–8.
- [6] R. R. Negenborn, M. Houwing, B. De Schutter, and J. Hellendoorn, "Model predictive control for residential energy resources using a mixed-logical dynamic model," in *Proc. Int. Conf. Netw. Sens. Control*, Okayama, Japan, pp. 702–707.
- [7] Z. Yi, D. Kullmann, A. Thavlov, O. Gehrke, and H. W. Bindner, "Active load management in an intelligent building using model predictive control strategy," in *Proc. IEEE PES PowerTech—Trondheim*, Trondheim, Norway, 2011, pp. 1–6.
- [8] A. Changsun, L. Chiao-Ting, and P. Huei, "Decentralized charging algorithm for electrified vehicles connected to smart grid," in *Proc. Amer. Control Conf.*, San Francisco, CA, USA, 2011, pp. 3924–3929.
- [9] L. W. Gan, U. Topcu, and S. H. Low, "Stochastic distributed protocol for electric vehicle charging with discrete charging rate," in *Proc. IEEE Power Energy Soc. Gen. Meeting*, San Diego, CA, USA, 2012, pp. 1–8.
- [10] Z. J. Ma, D. S. Callaway, and I. A. Hiskens, "Decentralized charging control of large populations of plug-in electric vehicles," *IEEE Trans. Control Syst. Technol.*, vol. 21, no. 1, pp. 67–78, Jan. 2013.
- [11] Z. Binyan, S. Yi, D. Xiaodai, L. Wenpeng, and J. Bornemann, "Short-term operation scheduling in renewable-powered microgrids: A duality-based approach," *IEEE Trans. Sustain. Energy*, vol. 5, no. 1, pp. 209–217, Jan. 2014.
- [12] S. Boyd, N. Parikh, E. Chu, B. Peleato, and J. Eckstein, "Distributed optimization and statistical learning via the alternating direction method of multipliers," *Found. Trends Mach. Learn.*, vol. 3, no. 1, pp. 1–122, 2011.
- [13] M. Kraning, E. Chu, J. Lavaei, and S. Boyd, "Message passing for dynamic network energy management," *Found. Trends Optim.*, vol. 1, no. 2, pp. 70–122, 2014.
- [14] A. Faruqui and S. Sergici, "Household response to dynamic pricing of electricity: A survey of the experimental evidence," Brattle Group, Cambridge, MA, USA, Tech. Rep., 2009.
- [15] J. Mattingley, Y. Wang, and S. Boyd, "Receding horizon control: Automatic generation of high-speed solvers," *IEEE Control Syst. Mag.*, vol. 31, no. 3, pp. 52–65, Jun. 2011.
- [16] J. Mattingley and S. Boyd, "CVXGEN: A code generator for embedded convex optimization," *Optim. Eng.*, vol. 13, no. 1, pp. 1–27, 2012.
- [17] Y. Wang and S. Boyd, "Performance bounds for linear stochastic control," *Syst. Control Lett.*, vol. 58, no. 3, pp. 178–182, 2009.
- [18] H. K. Alfares and M. Nazeeruddin, "Electric load forecasting: Literature survey and classification of methods," *Int. J. Syst. Sci.*, vol. 33, no. 1, pp. 23–34, 2002.
- [19] V. Dordonnata, S. J. Koopmanb, and M. Ooms, "Dynamic factors in periodic time-varying regressions with an application to hourly electricity load modelling," *Comput. Stat. Data Anal.*, vol. 56, no. 11, pp. 3134–3152, 2012.
- [20] *Energy Primer: A Handbook of Energy Market Basics*, Fed. Energy Regul. Comm., Washington, DC, USA, Jul. 2012.
- [21] T. Wang, H. Kamath, and S. Willard, "Control and optimization of grid-tied photovoltaic storage systems using model predictive control," *IEEE Trans. Smart Grid*, vol. 5, no. 2, pp. 1010–1017, Mar. 2014.
- [22] S. Boyd and L. Vandenberghe, *Convex Optimization*. Cambridge, U.K.: Cambridge Univ. Press, 2009.
- [23] *CAISO Market Reports*, CAISO, Folsom, CA, USA.
- [24] C. S. Chen, S. X. Duan, T. Cai, B. Y. Liu, and G. Z. Hu, "Optimal allocation and economic analysis of energy storage system in microgrids," *IEEE Trans. Power Electron.*, vol. 26, no. 10, pp. 2762–2773, Oct. 2011.
- [25] S. X. Chen, H. B. Gooi, and M. Q. Wang, "Sizing of energy storage for microgrids," in *Proc. IEEE Power Energy Soc. Gen. Meeting*, San Diego, CA, USA, 2012.
- [26] "Developing infrastructure to charge plug-in electric vehicles," Alternat. Fuels Data Center, U.S. Dept. Energy, Washington, DC, USA, Tech. Rep., Nov. 2013.
- [27] K. Clement-Nyns, E. Haesen, and J. Driesen, "The impact of charging plug-in hybrid electric vehicles on a residential distribution grid," *IEEE Trans. Power Syst.*, vol. 25, no. 1, pp. 371–380, Feb. 2010.
- [28] M. Alexander, "Puget sound regional council traffic choices study," Fed. Highway Admin., U.S. Dept. Transp., Washington, DC, USA, Tech. Rep., 2012.
- [29] M. Alexander and M. Davis, "Transportation statistics analysis for electric transportation," Elect. Power Res. Inst., Palo Alto, CA, USA, Tech. Rep. 1021848, Dec. 2011.
- [30] N. O'Connell, P. Pinsonb, H. Madsena, and M. O'Malley, "Benefits and challenges of electrical demand response: A critical review," Tech. Univ. Denmark, Lyngby, Denmark, Tech. Rep., 2013.
- [31] G. Wikler *et al.*, "The role of demand response in integrating variable energy resources," West. Interstate Energy Board, Denver, CO, USA, Tech. Rep., 2013.
- [32] K. Bullis, "Could electric cars threaten the grid?" *MIT Technol. Rev.*, 2013.

Authors' photographs and biographies not available at the time of publication.